



Laser micro/nano patterning of hydrophobic surface by contact particle lens array

Ashfaq Khan*, Zengbo Wang, Mohammad A. Sheikh, David J. Whitehead, Lin Li

Laser Processing Research Centre, School of Mechanical, Aerospace and Civil Engineering, The University of Manchester, Sackville Street, Manchester, M60 1QD, UK

ARTICLE INFO

Article history:

Received 31 May 2011

Received in revised form 17 August 2011

Accepted 22 August 2011

Available online 8 September 2011

Keywords:

Laser micro/nano patterning

Hydrophobic surface

CPLA

Optical near-field

ABSTRACT

Direct laser surface micro/nanopatterning by using Contact Particle Lens Array (CPLA) has been widely utilized. The method involves laser scanning of a monolayer of transparent particles arranged on the substrate to be patterned. Despite the different techniques available for CPLA deposition; the particles monolayer can only be formed on hydrophilic surfaces, which restrict the range of substrates that could be patterned by this method. In this study, a technique for patterning of hydrophobic surfaces by using CPLA has been proposed. In the proposed technique, monolayer of CPLA is formed on a hydrophilic substrate and then transported to a hydrophobic substrate by using a flexible sticky plastic. The transported CPLA is then scanned by a laser for patterning the hydrophobic substrate. The plastic pre-selected for this work was transparent to the laser. Experimental investigations were carried out to generate bumps and bowl shaped patterns using transported particles. Features smaller than the diffraction limit have been generated. The optical near field and associated temperatures around the particles were numerically simulated with a coupled electromagnetic and thermal modelling technique.

© 2011 Elsevier B.V. All rights reserved.

1. Introduction

Recent research into the enhancement of material properties by surface patterning has created an increased demand for new patterning techniques. Patterning has found applications in biomedical engineering, wettability improvement, friction and light absorption [1–4]. These widespread applications require robust manufacturing techniques, which could fabricate economically. There are many different techniques available for fabrication at nano scale but each has its limitations. Electron beam Lithography has a good feature size control and can provide a resolution of 10 nm but the technique is limited by low throughput and high sample cost [5]. X-ray lithography, on the other hand, has a high sample throughput but it is disfavoured because of its initial high capital cost [6]. Photolithography has been extensively used for fabrication because of its ease of repetition and capability of large area fabrication but the minimum feature size is limited by the diffraction limit [7–9].

Lasers have been widely used for submicron processing because of their unique advantages of being a non-contact process, capability of generating complicated structures without the need of photomask, ability to work in air, vacuum or water. Although the resolution of a laser is limited by the diffraction limit [10,11],

laser based near field techniques have been used to generate features smaller than the diffraction limit; features as small as 20 nm [7]. The commonly available near field techniques include Near-field Scanning Optical Microscope (NSOM) patterning [7,11,12], laser in combination with Scanning Probe Microscopy (SPM) for tip patterning [7,13] and plasmonic lithography [7,14]. Features with lateral dimensions below 30 nm have been generated by these techniques but they have not been adopted by industry because of their low throughput and difficulties with process control [15]. Recently, laser direct writing has been used to create complex 3D features with sub diffraction resolution. The process can reliably fabricate 3D features down to 100 nm lateral dimensions, even with commercially available equipment (<http://www.nanoscribe.de>, accessed July, 2011). However, the process is limited to the fabrication of di-electric polymeric structures with a low fabrication speed [16].

CPLA is one of the near field technique which has been extensively investigated in the last decade. The method originated from the material surface damage during dry laser cleaning [17]. In CPLA patterning method, spherical particles are spread over the substrate surface in the form of a monolayer and then scanned by laser. By laser interaction with the spherical particles, high intensity regions of evanescent waves are generated which are used for material processing [18]. This technique has been used to generate features on large as well as local areas both in air and while immersed in liquid [19,20]. In this method, the deposition of particles monolayer is a critically important step. There are many techniques available for the deposition of particles monolayer on a substrate including dip coating, spin coating and convective coating [21]. However, none of

* Corresponding author at: Zone E, D Floor, Pariser Building, School of Mechanical, Aerospace and Civil Engineering, The University of Manchester, P.O. Box 88, Manchester M60 1QD, UK. Tel.: +44 161 3062365/44 7940063327; fax: +44 0 161 306 3755.

E-mail address: Ashfaq.Khan@postgrad.manchester.ac.uk (A. Khan).

these methods could deposit monolayer of CPLA on a hydrophobic surface, which restricts the method to certain substrates and hence limits the widespread industrial applications [22].

In this study, a hydrophobic substrate was patterned by transporting a monolayer to a hydrophobic surface. A monolayer was first formed on a hydrophilic surface and then transferred to the hydrophobic surface by means of a flexible sticky plastic. The transported monolayer was then scanned by a laser in the usual conventional manner except that the laser passed through the supporting plastic. The generated features were characterized by Scanning Electron Microscope (SEM) and Atomic Force Microscope (AFM). The near field was numerically simulated by Finite Integration Technique (FIT) [23].

The purpose of this research work is to validate the technique for patterning of hydrophobic surfaces with features smaller than the diffraction limit. Patterning of a hydrophobic surface with CPLA was previously impossible because particles monolayer array could not be formed on it. With the proposed technique, the widespread industrial use of the CPLA technique for patterning of materials irrespective of their wetting properties could be realized. Patterning of curved surfaces has also been demonstrated recently with the proposed technique using particles of about 5 μm diameter but features smaller than the diffraction limit could not be created [24].

2. Experimental procedure

2.1. Materials

A silanized Silicon (Si) wafer with a contact angle of 110° was used as the hydrophobic substrate. The high contact angles were achieved by silanization with heptadecafluoro-trichlorosilane. Preparation of a monolayer generally requires the surface to have contact angle less than 20° . Drying of particles solution on Si led to the splitting of the solution in droplets and eventual formation of localized multilayer of particles. Si was selected because the technique was needed to be established for a high melting point material (Si melting point $\sim 1400^\circ\text{C}$).

In this work, silica particles (from Bangs Laboratories; diameter = $1\ \mu\text{m}$) were used for forming the monolayer array. A microscope glass slide (from Agar Scientific) was used as the hydrophilic surface for preparing the monolayer array. A Polypropylene plastic (of thickness $45\ \mu\text{m}$) coated with acrylic based adhesive resin (thickness $0.5\ \mu\text{m}$) was used for transporting CPLA (referred to as the 'Ribbon'). The ribbon had transmission above 90% at 532 nm.

2.2. Equipment

A 532 nm Nd:YVO₄ laser (Laserline-Laserval Violino pulse duration of $\tau = 7\ \text{ns}$, frequency = 1–30 kHz, S-polarized) was used as the irradiation source. A computer controlled galvo-scanning system controlled the laser beam movement. Characterization of samples was conducted by Scanning Electron Microscope (SEM, Hitachi High Technologies, S-3400N), and Atomic Force Microscope (AFM, Veeco Innova). A spectrophotometer (Analytik Jena) was used for measuring the optical properties of the ribbon.

2.3. CPLA monolayer preparation and transportation

A monolayer of particles was formed on a hydrophilic glass surface, which was then transported to the Si surface. For forming monolayer, the glass slide was first cleaned by soapy water. It was sonicated first in acetone and then in methanol for 10 min each. Finally, it was rinsed with de-ionized water and dried in a flow of nitrogen gas. Finally, it was treated with an aqueous solution of nitric acid to make it hydrophilic [25]. The monolayer of CPLA

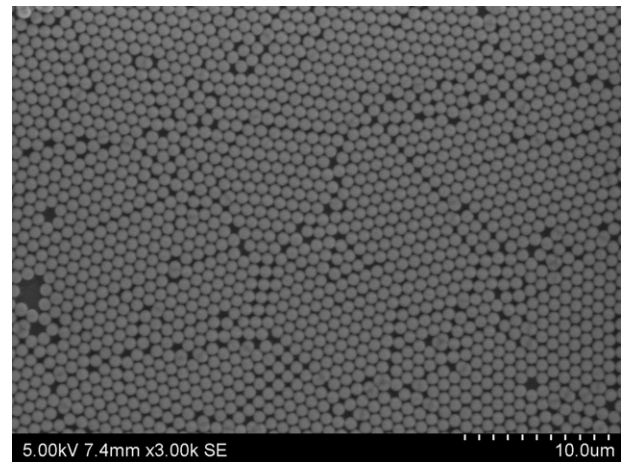


Fig. 1. SEM image of $1\ \mu\text{m}$ particles monolayer array.

was prepared by spreading a diluted solution of contact particles on glass. The substrate was dried in an airtight box and placed at a small angle (9°) for ease of particles nucleation [26]. As the solution dried, the particles arranged themselves in a hexagonal closed pack array due to capillary forces [27]. SEM image of the generated monolayer is shown in Fig. 1.

For transporting the monolayer, the ribbon was positioned above the particles monolayer and pressed gently to secure the particles to the ribbon. The ribbon with the attached monolayer of CPLA was then lifted and placed over the Si surface. In this manner, the hydrophobic surface was effectively covered by a CPLA monolayer. The procedure for transporting CPLA is schematically represented in Fig. 2. The Si surface covered by ribbon before laser processing is shown in Fig. 3.

3. Results and discussion

3.1. Laser processing

A 532 nm Nd:YVO₄ laser was used as the irradiation source. The experimental setup is shown in Fig. 4. A defocused beam (having large divergence angle) with a spot size of about $65\ \mu\text{m}$ diameter, scan speed of 1 m/s, repetition rate of 30 kHz and pulse duration of $\tau = 7\ \text{ns}$ was used for processing. These processing parameters ensured that none of the sample was left without laser illumination. All the experiments were carried out under ambient conditions. During laser irradiation, laser beam passed through the ribbon to pattern the substrate. The transmission of laser through the ribbon was achieved by a careful selection of ribbon material and laser type. The ribbon with transmission above 90% at 532 nm enabled the laser beam to pass through the ribbon without damaging it and facilitated the use of maximum laser intensity for patterning.

With fluence in the range of $0.947\ \text{J}/\text{cm}^2$ to $2.47\ \text{J}/\text{cm}^2$, features were generated on the substrate. The laser was able to pass through the ribbon without damaging it and after intensity enhancement by the particles, it was able to generate features on the substrate. At a fluence of $2.47\ \text{J}/\text{cm}^2$, bowl shaped patterns with lateral dimensions of $220 \pm 10\ \text{nm}$ were generated, as shown in Fig. 5a. The depth of features measured by AFM was found to be about $20 \pm 1\ \text{nm}$. With reduction in laser fluence, the bowl shaped patterns changed into a mix of bump and bowl shaped features. With continued reduction in laser fluence to about $0.947\ \text{J}/\text{cm}^2$ large area bump shaped features were generated with lateral dimension of about $160 \pm 10\ \text{nm}$, as shown in Fig. 5b. The height of the bumps was measured to be $8 \pm 1\ \text{nm}$. The shape of the features remained the same with further reduction in laser fluence until $0.379\ \text{J}/\text{cm}^2$ when the bump

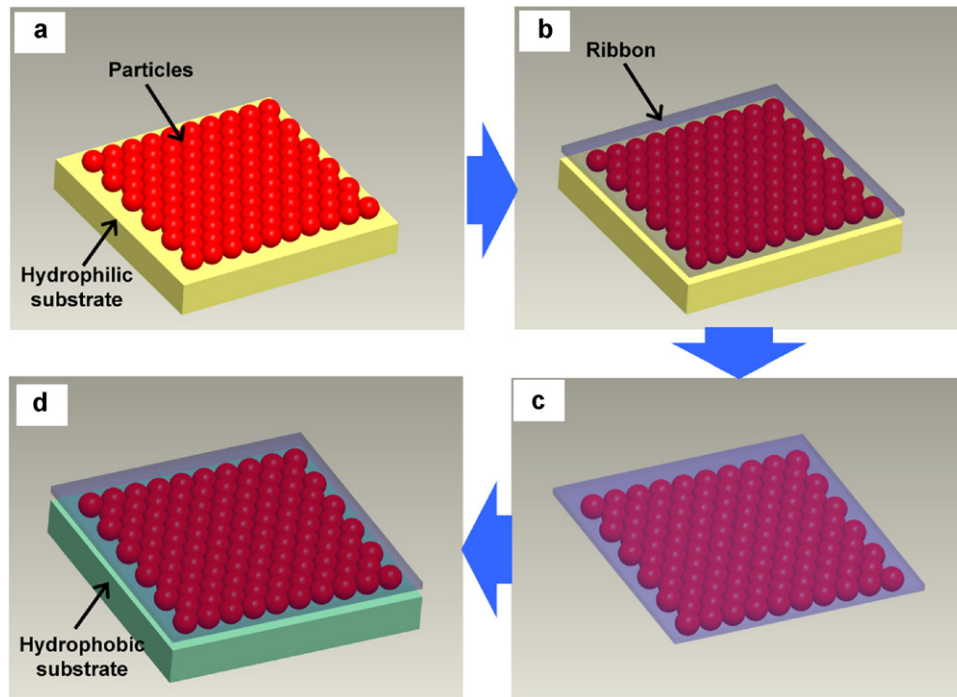


Fig. 2. A schematic representation of the transfer of particles. (a) Monolayer of CPLA formed on glass (b) CPLA secured by a ribbon (c) CPLA is lifted from the glass surface by the ribbon (d) CPLA is transferred to the hydrophobic surface.

shaped patterns started to disappear and only amorphization of Si was observed, as shown in Fig. 5c. The amorphization took place because the intensity enhancement by particles was insufficient to ablate Si. The interspacing between the features at all fluence values was observed as about $1\ \mu\text{m}$, which related closely with the diameter of the particles used. Features with dimensions in the range of $160\text{--}220\ \text{nm}$ were generated which are smaller than the diffraction limit of $266\ \text{nm}$. The experiments were repeated in argon to study the effect of environment. The results were found to be similar as in air. The effect of argon was negligible because the ribbon provided a partition between the environment and near field processing.

3.2. Near field modelling

The optical near-fields around silica particles (refractive index $=\eta_{\text{Silica}} = 1.46$ at $532\ \text{nm}$) and on Si (refractive

index $=\eta_{\text{Silicon}} = 4.15 + 0.043933i$ at $532\ \text{nm}$) were simulated using a commercially available software (CST Microwave studio) [28]. The incident beam used was s-polarized. The dielectric constants for the particle and the substrate were 2.1316 and 17.22056, respectively. The model is shown in Fig. 6. The particles were secured by the resin (refractive index $=\eta_{\text{resin}} = 1.4947$ and extinction coefficient $=k=0$) and the Si surface was covered by a $2\ \text{nm}$ thick layer of a naturally occurring oxide. The Si substrate was taken to be about $2\ \mu\text{m}$ thick to cater for the deep optical penetration of the $532\ \text{nm}$ laser, which is plotted in Fig. 7. The y-axis of Fig. 7 shows the ratio of intensity at a certain depth (I) to the incident intensity (I_0). At a depth of $2\ \mu\text{m}$, 90% of the incident intensity is absorbed by Si. The optical penetration depth is calculated by using the Beer Lambert law [29].

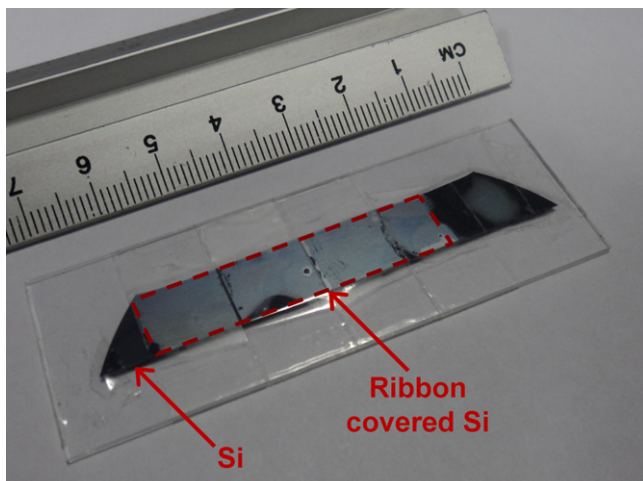


Fig. 3. Si surface covered by ribbon before laser processing.

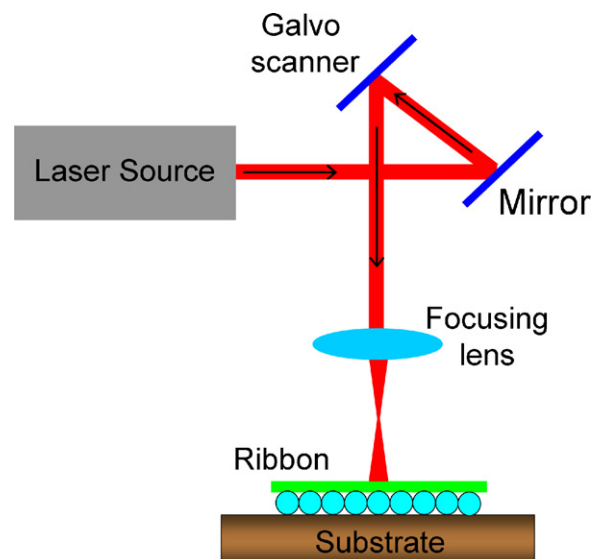


Fig. 4. Experimental setup.

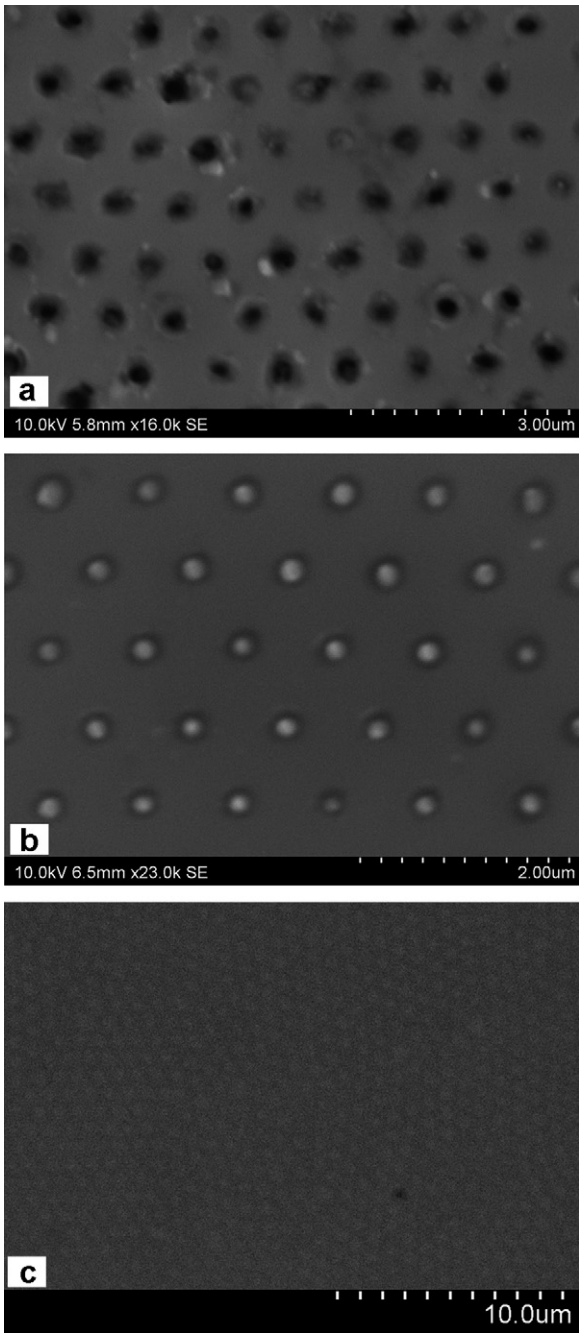


Fig. 5. SEM images of features (a) bowl shaped patterns generated at 2.47 J/cm², (b) bumped shaped patterns generated at 0.947 J/cm², (c) bumped shaped patterns generated at 0.379 J/cm².

The modelling was carried for a Gaussian pulse with pulse duration of 7 ns. The maximum intensity enhancement in the near field on the substrate is shown in Fig. 8. For particles on Si surface, an intensity enhancement of 5.61 times was calculated. For a 7 ns Gaussian pulse, the highest intensity enhancement was achieved at about 5 ns. It is well documented that for a normally incident laser the intensity enhancement under the particle has a Gaussian distribution [13], which is reasserted in this case. The Gaussian intensity distribution can be used to generate features of varying dimension by controlling laser fluence [30].

The simulated intensity enhancement was used for calculating temperatures under a particle at different values of a laser fluence. The simulation was carried out for 15 ns for understanding the

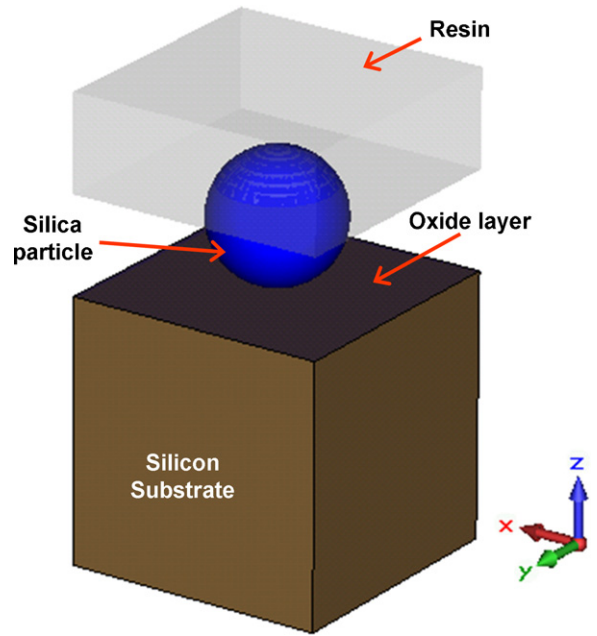


Fig. 6. Model of a single particle on Si and partially submerged in resin.

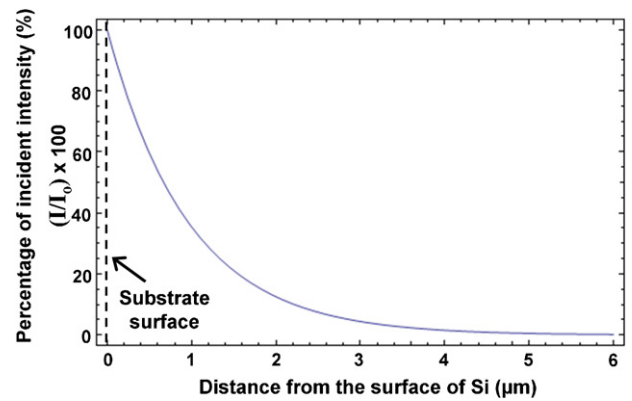


Fig. 7. Absorption of laser intensity with depth of substrate.

decay of the intensity and associated temperatures at the end of the pulse. For a 7 ns pulse, the highest temperatures from the simulation (using CST Microwave studio) are summarized in Table 1. The temperature distribution for a fluence of 0.947 J/cm² is shown in Fig. 9.

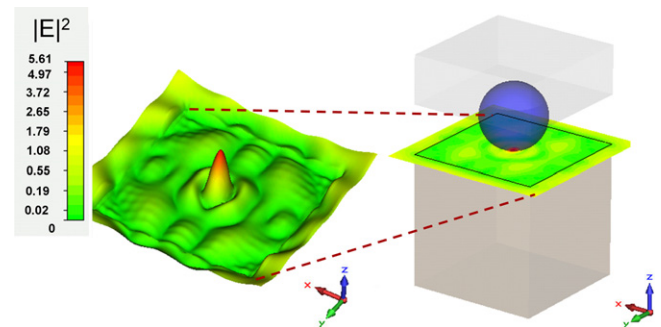


Fig. 8. Maximum Intensity field distribution for a 1 μm particle under a normal incident beam.

Table 1
Temperatures simulated at different fluence and features generated during experimentation.

S. no	Laser fluence (J/cm ²)	Maximum temperature by modelling (K)	Features generated by experimentation
1	2.47	2895	Bowl shaped
2	0.947	2049	Bump shaped
3	0.379	1340	No features generated – only amorphization

3.3. Hydrodynamic mechanism of feature formation

The generation of features on the substrate can be explained on the basis of melt pool flows and ablation of material. In the melt pool there are two basic internal flows; Marangoni flows induced by surface tension gradients, and by gravity force [31]. The gravitational forces are insignificant at nanometre scale and thus Marangoni flows and ablation of material are responsible for the shape formation [15,32]. The basis of Marangoni flow is that surfaces with high surface tension pull the surrounding liquid more strongly than surfaces with low surface tension. The difference in pull causes flow of material that is responsible for the formation for features upon solidification of the melt pool region. Marangoni flow has two distinct components; Thermo-capillarity (Thermo-capillary force), and Chemi-capillarity (Chemi-capillary force), caused by temperature and material gradients respectively [31].

Near field modelling shows that the intensity distribution is nearly Gaussian. The Gaussian intensity distribution induces a variation in temperature, which causes surface tension gradient and hence induces Thermo- capillarity (Marangoni flow). Although pure Si (99.999% pure) is used in this study, the presence of naturally occurring oxide layer can also act as surfactant above certain fluence of laser [15].

At fluence of 0.379 J/cm² only amorphization of Si occurs [19]. From the near field analysis, the predicted temperature is 1340 K, which is much below the melting point of Si. As a result, there is no material melting or ablation and hence no patterning. For laser fluence above 0.947 J/cm², bump shaped patterns were observed on the substrate. The temperature generated at this fluence is 2049 K, which is higher than the melting temperatures of Si and SiO₂ oxide layer but lower than the ablation threshold for Si. The generation of these bump shaped patterns suggest an inward flow that forms the bump in the centre. The inward flow is induced by chemi-capillary Marangoni flow. The high laser intensity in the centre of the Gaussian optical field enhancement induces a concentration gradient by the melting of the surface oxides which causes the inward flow [15,33]. The inward flow of material upon cooling forms the bump shaped feature. At fluence of 2.47 J/cm², with temperature of 2895 K, the shape of the feature changes into a bowl

shaped structure with an outer rim. The structure is formed due to the strong ablation in the centre.

3.4. Advantages of de focused beam

A defocused laser beam was used to improve the distribution of the generated features. With focused laser beam the features were not in a perfect hexagonal distribution. Under a focused laser beam high temperatures were generated in a small region between the ribbon and the substrate. These high temperatures displaced of the neighbouring particles from their position, which caused the features to be generated in a non-perfect hexagonal closed shaped array. With defocused laser, there is no concentration of energy, and particles stay in their position resulting in a good distribution of structures. Moreover, a defocused beam enables the processing of larger areas thus increasing the speed of patterning.

3.5. Repeatable use of particles

With the method presented in this paper, the particles monolayer can be reused several times. Similar results are produced when a particles monolayer is reused. The results are nearly identical with repetition of up to three times. Similar bumps and bowl shaped patters are generated within the above mentioned range of fluence. The reason for the repeatable use of the monolayer to be possible was that the ribbon possessed more than 90% transmission under the laser wavelength. Also, the adhesive held the particles firmly, which made the repeatable use possible. For repetition beyond three times, a very small number of particles were lost from the ribbon with every successive use.

4. Conclusions

The successful patterning of a high melting point, hydrophobic surface with 110° contact angle has shown that the technique could be extended to patterning of most commonly available materials. Moreover, the technique does not require long waiting periods for drying of the particles solution on the surfaces to be patterned.

In summary, a new technique for micro/nano patterning has been proposed which is simple, fast, allows large area monolayer arrays to be transported, does not require a perfect monolayer, is independent of particle material, and can be applied to surfaces irrespective of their wettability. In this technique, a conventional procedure is used to produce a monolayer of CPLA. A transparent, flexible plastic with adhesive is used to peel the CPLA and transport it to the hydrophobic surface. Irradiation of the hydrophobic surface with a laser passing through the plastic and focused by micro particles makes the patterning of hydrophobic surface possible.

Acknowledgements

The corresponding author (A. Khan) gratefully acknowledges the support from the NWFP, University of Engineering and Technology (UET), Pakistan. The authors would also like to thank the staff and members of the Laser Processing Research Centre (LPRC), University of Manchester, UK, for their support.

References

- [1] A. Pena, Z.B. Wang, D. Whitehead, L. Li, High speed laser micro-texturing of Si wafer for improved light trapping for photo-voltaic application, in: 28th International Congress on Applications of Lasers & Electro-Optics (ICALEO), Orlando, FL, USA, 2009.
- [2] A. Kietzig, S.G. Hatzikiriakos, P. Englezos, Patterned superhydrophobic metallic surfaces, *Langmuir* 25 (8) (2009) 4821.
- [3] J. Xuan, S. Chung, P. Zhengda, T. Nguyen, Y. Shel, Optimization of bump shape and pattern in laser-texture design for improving media tribological performances, *Magn. IEEE Trans.* 35 (5) (1999) 2436.

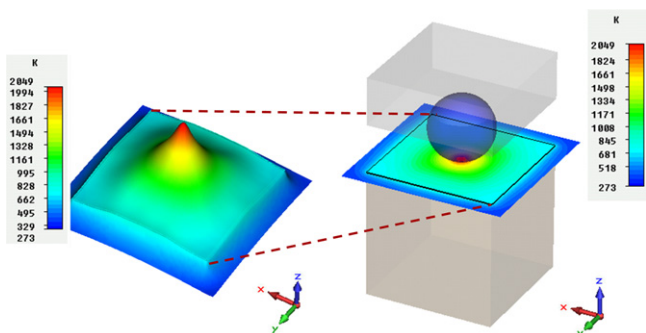


Fig. 9. Temperature under the particle at 5 ns for a laser fluence of 0.947 J/cm².

- [4] N. Gadegaard, E. Martines, M.O. Riehle, K. Seunarine, C.D.W. Wilkinson, Applications of nano-patterning to tissue engineering, *Microelectron. Eng.* 83 (2006) 1577.
- [5] K. Liu, P. Avouris, J. Bucchignano, R. Martel, S. Sun, J. Michl, Simple fabrication scheme for sub-10 nm electrode gaps using electron-beam lithography, *Appl. Phys. Lett.* 80 (5) (2002) 865.
- [6] H.I. Smith, M.L. Schattenburg, X-Ray-lithography, from 500 to 30 nm – X-ray nanolithography, *IBM J. Res. Dev.* 37 (3) (1993) 319.
- [7] T.C. Chong, M.H. Hong, L.P. Shi, Laser precision engineering: from microfabrication to nanoprocessing, *Laser Photon Rev.* 4 (1) (2010) 123.
- [8] T. Ito, S. Okazaki, Pushing the limits of lithography, *Nature* 406 (6799) (2000) 1027.
- [9] J.E. Bjorkholm, J. Bokor, L. Eichner, R.R. Freeman, J. Gregus, T.E. Jewell, W.M. Mansfield, A.A. Mac Dowell, E.L. Raab, W.T. Silfvast, L.H. Szeto, D.M. Tennant, W.K. Waskiewicz, D.L. White, D.L. Windt, O.R. Wood, J.H. Bruning, Reduction imaging at 14 nm using multilayer coated optics: printing of features smaller than 0.1 μm , *J. Vac. Sci. Technol. B* 8 (6) (1990) 1509.
- [10] E. Abbe, Theorie des Mikroskops und der mikroskopischen Wahrnehmung, *Arch. Mikroskop. Anat.* 9 (1873) 413.
- [11] E. Betzig, J.K. Trautman, Near-field optics—microscopy, spectroscopy, and surface modification beyond the diffraction limit, *Science* 257 (5067) (1992) 189.
- [12] E. Betzig, J.K. Trautman, R. Wolfe, E.M. Gyorgy, P.L. Finn, M.H. Kryder, C.H. Chang, Near-field magneto-optics and high density data storage, *Appl. Phys. Lett.* 61 (2) (1992) 142.
- [13] Y.F. Lu, Z.H. Mai, Y.W. Zheng, W.D. Song, Nanostructure fabrication using pulsed lasers in combination with a scanning tunneling microscope: mechanism investigation, *Appl. Phys. Lett.* 76 (9) (2000) 1200.
- [14] Z. Liu, Q. Wei, X. Zhang, Surface plasmon interference nanolithography, *Nano Lett.* 5 (5) (2005) 957.
- [15] Y. Lu, S.C. Chen, Nanopatterning of a silicon surface by near-field enhanced laser irradiation, *Nanotechnology* 14 (5) (2003) 505.
- [16] G.V. Freymann, A. Ledermann, M. Thiel, I. Staude, S. Essig, K. Busch, M. Wegener, Three-dimensional nanostructures for photonics, *Adv. Funct. Mater.* 20 (2010) 1038.
- [17] M. Mosbacher, H.J. Munzer, J. Zimmermann, J. Solis, J. Boneberg, P. Leiderer, Optical field enhancement effects in laser-assisted particle removal, *Appl. Phys. A: Mater. Sci. Process.* 72 (2001) 41.
- [18] W. Guo, Z.B. Wang, L. Li, D.J. Whitehead, B.S. Luk'yanchuk, Z. Liu, Near-field laser parallel nanofabrication of arbitrary-shaped patterns, *Appl. Phys. Lett.* 90 (24) (2007) 243101.
- [19] A. Pena, et al., Laser generation of nano-bumps below 2 nm height on silicon for debris-free marking/patterning, *J. Phys. D: Appl. Phys.* 43 (11) (2010) 115302.
- [20] W. Guo, Z.B. Wang, L. Li, Z. Liu, B. Luk'yanchuk, D.J. Whitehead, Chemical-assisted laser parallel nanostructuring of silicon in optical near fields, *Nanotechnology* 19 (45) (2008) 4.
- [21] Y.H. Wang, W.D. Zhou, A review on inorganic nanostructure self-assembly, *J. Nanosci. Nanotechnol.* 10 (3) (2010) 1563.
- [22] F. Burmeister, C. Schafle, B. Keilhofer, C. Bechinger, B. Johannes, L. Paul, From mesoscopic to nanoscopic surface structures: lithography with colloid monolayers, *Adv. Mater.* 10 (6) (1998) 495.
- [23] Z.B. Wang, B.S. Luk'yanchuk, W. Guo, S.P. Edwardson, D.J. Whitehead, L. Li, Z. Liu, K.G. Watkins, The influences of particle number on hot spots in strongly coupled metal nanoparticles chain, *J. Chem. Phys.* 128 (9) (2008) 094705.
- [24] A. Khan, Z. Wang, M. Sheikh, D. Whitehead, L. Li, Parallel near-field optical micro/nanopatterning on curved surfaces by transported micro-particle lens arrays, *J. Phys. D: Appl. Phys.* 43 (30) (2010) 305302.
- [25] Z.B. Wang, W. Guo, A. Pena, D.J. Whitehead, B.S. Luk'yanchuk, L. Li, Z. Liu, Y. Zhou, M.H. Hong, Laser micro/nano fabrication in glass with tunable-focus particle lens array, *Opt. Express* 16 (24) (2008) 19706.
- [26] R. Micheletto, H. Fukuda, M. Ohtsu, A simple method for the production of a two-dimensional, ordered array of small latex particles, *Langmuir* 11 (9) (2002) 3333.
- [27] N. Denkov, O. Velev, P. Kralchevski, I. Ivanov, H. Yoshimura, K. Nagayama, Mechanism of formation of two-dimensional crystals from latex particles on substrates, *Langmuir* 8 (12) (1992) 3183.
- [28] E.D. Palik, *Handbook of Optical Constants of Solids*, Academic Publisher, New York, 1998, ISBN 0-12-544420-6.
- [29] D. Bäuerle, *Laser Processing and Chemistry*, Springer, 2000, ISBN 978-3540605416.
- [30] F. Korte, J. Serbin, J. Koch, A. Egbert, C. Fallnich, A. Ostendorf, B.N. Chichkov, Towards nanostructuring with femtosecond laser pulses, *Appl. Phys. A: Mater. Sci. Process.* 77 (2003) 229.
- [31] C. Limmaneevichitr, S. Kou, Experiments to simulate effect of Marangoni convection on weld pool shape, *Weld. J.* 79 (2000) 231s.
- [32] Y. Lu, S. Theppakuttai, S.C. Chen, Marangoni effect in nanosphere-enhanced laser nanopatterning of silicon, *Appl. Phys. Lett.* 82 (23) (2003) 4143.
- [33] Z.B. Wang, M.H. Hong, B.S. Luk'yanchuk, S.M. Huang, Q.F. Wang, L.P. Shi, T.C. Chong, Parallel nanostructuring of GeSbTe film with particle mask, *Appl. Phys. A: Mater. Sci. Process.* 79 (4) (2004) 1603.